Nanoscale

PAPER

View Article Online
View Journal | View Issue

Cite this: *Nanoscale*, 2014, **6**, 6609

Covalently functionalized carbon nanotube supported Pd nanoparticles for catalytic reduction of 4-nitrophenol†

Xianmo Gu,[ab] Wei Qi,[b] Xianzhu Xu,*[a] Zhenhua Sun,*[b] Liyun Zhang,[b] Wei Liu,[b] Xiaoli Pan[b] and Dangsheng Su*[b]

Received 14th February 2014
Accepted 25th March 2014

DOI: 10.1039/c4nr00826j

www.rsc.org/nanoscale

Carbon nanotubes (CNTs) were covalently functionalized *via* 1,3-dipolar cycloaddition reaction under microwave conditions. The functionalized CNTs were characterized by thermogravimetric analysis (TGA), X-ray photoelectron spectroscopy (XPS), N_2 adsorption isotherms and Raman spectroscopy. The surface concentration of phenolic hydroxyl groups on the surface of CNTs was adjusted by varying the reaction temperature. In addition, we prepared Pd nanoparticle/CNT (Pd NP/CNT) nanocomposites through strong electrostatic adsorption and hydrogen reduction. The results indicated that the functional groups could not only improve the dispersion of CNTs in water, but also enhance the interaction between Pd precursors and CNTs, thus preventing small Pd NPs (average diameter of 1.5 nm) from agglomerating. Furthermore, the Pd NP/CNT-220 nanocomposites showed high catalytic activity for the reduction of 4-nitrophenol. The turnover frequency (TOF) of this catalyst was up to 18 min^{-1}, which was attributed to the small size and uniform distribution of Pd NPs on the surface of CNTs.

Introduction

Noble metal nanoparticles (NPs) are favored in various reactions such as hydrogenation, dehydrogenation and oxidation.[1] However, the extremely high price and rare resource limit their large scale applications. Therefore, it is of paramount importance to improve the utilization efficiency of noble metals. Nanocarbon materials supported noble metal NPs have recently attracted considerable attention in various fields of chemistry and engineering, and it is proven to be an efficient method to solve these problems.[2] The high thermal stability and excellent structural, electrical, and mechanical properties enable carbon nanotubes (CNTs) to be fascinating support materials.[3] However, the intrinsic poor-solubility of pristine CNTs due to their chemically inert surfaces greatly hinders their utilization, including dispersion in solutions and bonding to other materials.[4] Chemical functionalization has been proven to be a key approach to overcome this problem. The main approaches to functionalize CNTs can be classified into two categories: non-covalent functionalization with various organic molecules through van der Waals or π–π interactions and covalent functionalization through chemical bonds.[5] It has been reported that CNTs could be non-covalently functionalized with 1-pyrenemethanol initiated hyperbranched polyglycerol (PiHP), and then various metal NPs can be attached onto CNTs to form nanocomposites.[2c] Although this method increased the dispersion of CNTs in water, the π–π interactions between CNTs and functional molecules were weaker than chemical bonds, as a result, the nanocomposites were relatively unstable. In order to improve the stability, CNTs were functionalized through a covalent approach, and two main methods have been developed so far. CNTs are oxidized under strong acidic conditions and then react with alcohols or amines to form ester or amide derivatives. For example a method to fabricate thiol-functionalized CNTs has been reported, which was used for the immobilization of Pt NPs at high loadings. In this method, the CNTs were first oxidized by nitric acid (HNO_3), followed by chlorination with thionyl chloride ($SOCl_2$), and then reacted with 4-aminothiophenol.[6] The dispersion of CNTs and the stability of the catalyst were improved, whereas this experimental process was tedious and intricate. Furthermore, it is difficult to control the type and concentration of functional groups on the surface of CNTs by HNO_3 oxidation. Another commonly used method is that CNTs are functionalized through addition reactions, such as nucleophilic addition, free-radical addition, cycloaddition, and Birch reduction and reductive alkylation.[5] Among these addition reactions, 1,3-dipolar cycloaddition plays a very important role in forming novel hybrid materials, especially Prato reactions.[7] These methods could be used to obtain CNTs

[a]*State Key Laboratory of Urban Water Resource and Environment, Harbin Institute of Technology, Harbin 150090, P. R. China. E-mail: xuxianzhu@hit.edu.cn; Fax: +86 451 86403625; Tel: +86 451 86403715*

[b]*Shenyang National Laboratory for Materials Science, Institute of Metal Research, Chinese Academy of Sciences, 110016 Shenyang, P. R. China. E-mail: zhsun@imr.ac.cn; dssu@imr.ac.cn; Fax: +86 24 83970019; Tel: +86 24 83978238*

† Electronic supplementary information (ESI) available. See DOI: 10.1039/c4nr00826j

with single type of functionalities, but a long reaction time and low yield hamper their large scale applications. Microwave synthesis is an effective way to improve the efficiency of the reaction.[8] Here, we have firstly developed a facile method for functionalizing CNTs with *N*-methylglycine and 3,4-dihydroxybenzaldehyde under microwave radiation *via* 1,3-dipolar cycloaddition. This method not only improves the dispersion of CNTs in solvent, but also ensures only one type of functional group (phenolic hydroxyl groups) on the surface of CNTs. Then, Pd^{2+} ions were adsorbed onto the functionalized CNTs through strong electrostatic interactions; after the H_2 reduction Pd NP/CNT nanocomposites could be fabricated. The average size of Pd NPs was around 1.5 nm, and the nanocomposites showed high catalytic activity in the reduction of 4-nitrophenol. The TOF of this catalyst was up to 18 min^{-1}, which was attributed to the small size and uniform distribution of Pd NPs on the surface of CNTs.

Experimental section

Materials

The multiwall carbon nanotubes (FloTube 9000) were obtained from CNano Technology Limited Company, China. *N*-Methylglycine and 12 wt% palladium nitrate ($Pd(NO_3)_2$) solution were purchased from Alfa Aesar; 3,4-dihydroxybenzaldehyde, dimethylformamide (DMF), ethanol, 4-nitrophenol, sodium borohydride ($NaBH_4$) and sodium carbonate (Na_2CO_3) were obtained from Sinopharm Chemical Reagent Co., Ltd, China. All chemicals were of analytical grade and were used as received without further purification.

Purification and oxidation of CNTs

CNTs were dispersed in concentrated hydrochloric acid by ultrasonication for 15 min and then stirred at room temperature for 24 h. After treatment, the solution was filtered and the sample was thoroughly rinsed with deionized water until the pH value reached 6–7. The resulting black solid was dried in a vacuum oven at 100 °C overnight. Then, the CNTs were transferred into a fixed bed quartz glass tube reactor operating at atmospheric pressure and heated at 1000 °C for 5 h under an argon flow (100 mL min^{-1}). The resulting sample was labeled NF-CNT. The NF-CNT was refluxed in concentrated HNO_3 at 120 °C for 2 h. After filtering and washing until pH = 6–7, the final product is denoted as O-CNT.

Functionalization of CNTs

The experiments were performed in a Questron Microwave Digestion System (QLAB 8000) with sensor vessels and standard digestion vessels. The CNTs, *N*-methylglycine and 3,4-dihydroxybenzaldehyde were dispersed in DMF by ultrasonication for 30 min and then placed inside a microwave oven. The mixture was heated to the target temperature and kept for 30 min. The target temperature was 160 °C, 200 °C and 220 °C, respectively. When the vessel was cooled to room temperature, the product was filtered using a sand core funnel. Then the product was washed with DMF and ethanol by ultrasonication and filtration until the filtrate was clear. The resulting black sample was dried in a vacuum oven at 100 °C overnight. The functionalized CNTs are denoted as CNT-*X*, where *X* is the reaction temperature.

Preparation of 2 wt% Pd NP/CNT nanocomposites

Firstly, 25 μL of $Pd(NO_3)_2$ solution (0.016 g mL^{-1}) was added to 5 mL deionized water. Then, the pH of this solution was adjusted to 4–5 using Na_2CO_3 solution (0.2 M). Secondly, 20 mg of CNTs was added to the above solution, the mixture was ultrasonicated for 1 h and then stirred at room temperature overnight. Then, the mixture was filtered, washed and dried. Finally, the dried product was reduced by H_2 at 200 °C for 2 h.

Catalytic reduction of 4-nitrophenol

In a typical reduction reaction, 2 mL of 4-nitrophenol aqueous (5×10^{-5} M) and 1 mL of fresh $NaBH_4$ solution (0.05 M) were added to a quartz cuvette, then 100 μL of catalyst (0.05 g L^{-1}) aqueous solution was added to the quartz cuvette. The reaction was monitored *in situ* using UV/vis spectroscopy.

Characterization

Thermogravimetric analysis (TGA) was performed on a NETZSCH STA 449 F3 under a flow of argon (50 mL min^{-1}) with a heating rate of 10 °C min^{-1} from 35 to 950 °C. The X-ray photoelectron spectroscopy (XPS) measurements were carried out using an ultra-high vacuum (UHV) ESCALAB 250 set-up equipped with a monochromatic Al Kα X-ray source (1486.6 eV; anode operating at 15 kV and 20 mA). The peak was calibrated based on the C 1s peak of graphitic carbon (284.6 eV). The XPS spectra were fitted using mixed Gaussian–Lorentzian component profiles (at a ratio of 80/20 – 60/40) after subtraction of a Shirley background using XPSPEAK41 software. The specific surface area was measured by the Brunauer–Emmett–Teller (BET) method using nitrogen adsorption–desorption isotherms on a Micrometrics ASAP 3020 system. Raman spectroscopy was performed on a LabRam HR 800 using a 633 nm laser. UV-vis spectra of the samples were obtained using a Cary 5000 UV/vis/NIR spectrophotometer. The elemental analysis was performed using an inductively coupled plasma-atomic emission spectrometer (ICP-AES, IRIS Intrepid). The morphology of the samples was characterized using a transmission electron microscope (FEI-T12 and FEI-F20). Zeta potentials of the samples were measured using a Malvern zeta meter (Zetasizer 2000).

Results and discussion

In order to exclude the effects of amorphous carbon and metal impurities, CNTs were pretreated with acid and calcined at high temperature before the functionalization. As shown in Fig. 1, the quantity of amorphous carbon on CNTs decreased after pretreatment, which was beneficial to the functionalization process.

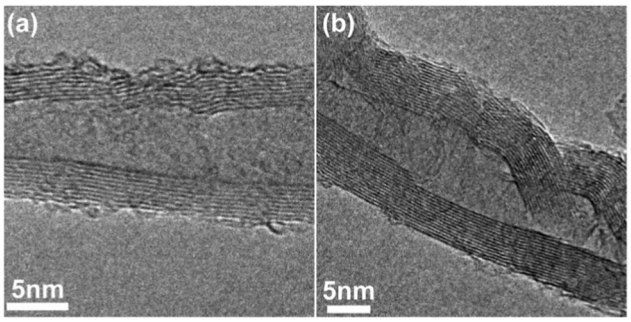

Fig. 1 The TEM images of CNTs before (a) and after (b) the pre-treatment.

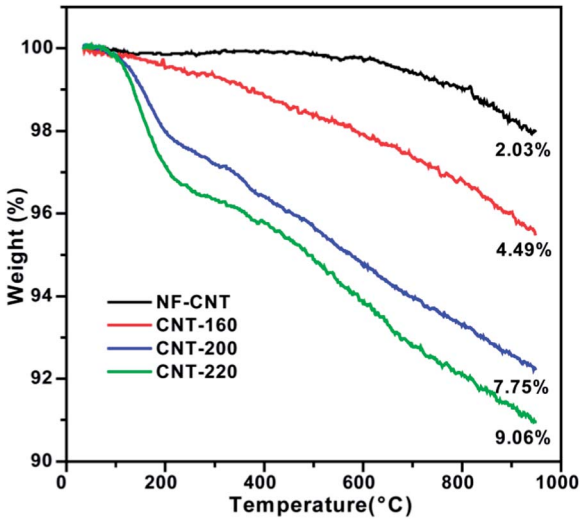

Fig. 3 The TGA curves of non-functionalized and functionalized CNTs under argon flow.

Functionalization of CNTs

It is reported that microwave is beneficial to the functionalization of CNTs *via* 1,3-diploar cycloaddition by improving the reaction selectivity and reducing the reaction time.[8] It took five days when this reaction was carried out through conventional methods.[7] In contrast, the microwave-assisted reaction could be completed within 30 min, as shown in Fig. 2. The CNTs were functionalized with *N*-methylglycine and 3,4-dihydroxybenzaldehyde under microwave radiation *via* 1,3-dipolar cycloaddition. The degree of functionalization was adjusted by changing the reaction temperature. Furthermore, the structure of the functionalized CNTs was thoroughly characterized by TGA, XPS, N_2 adsorption and Raman spectroscopy.

TGA studies performed under an inert atmosphere could provide the information on the weight content of organic groups functionalized on CNTs and the results are presented in Fig. 3 and Table 1. According to the values 2.03%, 4.49%, 7.75% and 9.06%, an enhancement of weight loss (Δm, wt%) was calculated over all functionalized CNTs with respect to the non-functionalized ones, which increased as the reaction temperature increased, indicating that CNTs were successfully functionalized. The functional groups on the surface of CNTs increased with increasing reaction temperature.

XPS is usually used to analyze the loading content and surface structure of functionalized CNTs. As shown in Table 1, comparing with the non-functionalized CNTs, the existence of nitrogen species in the functionalized CNTs confirmed the success of the 1,3-dipolar cycloaddition reaction performed on CNTs. The nitrogen and oxygen amounts in the functionalized CNTs increased with the increase of reaction temperature. Moreover, the N 1s spectra could also provide quantitative information about the functional groups based on the peak area. Fig. 4 presents the curve fitted N 1s XPS of non-functionalized and functionalized CNTs. The binding energy of N1 was about 400.8 eV corresponding to nitrogen atoms in carbamate bonds (similarly pyrrole), which was obtained *via* the 1,3-dipolar cycloaddition reaction.[4a,9] The N2 species, exhibiting a lower binding energy of about 399.7 eV, may be ascribed to amide groups.[10] Meanwhile, the curve fitted C 1s and O 1s XPS of non-functionalized and functionalized CNTs could indicate that the functionalization was successfully performed on CNTs. The carbon species were divided into five peaks: sp^2 C=C (284.6 eV, C1), C–OH (286.1 eV, C2), C=O (287.5 eV, C3), O=C–O (289.5 eV, C4), and π–π^* (291.4 eV, C5), and the oxygen species were divided into three peaks: C=O (531.2 eV, O1), O=C–O (532.4 eV, O2), and C–OH (533.9 eV,

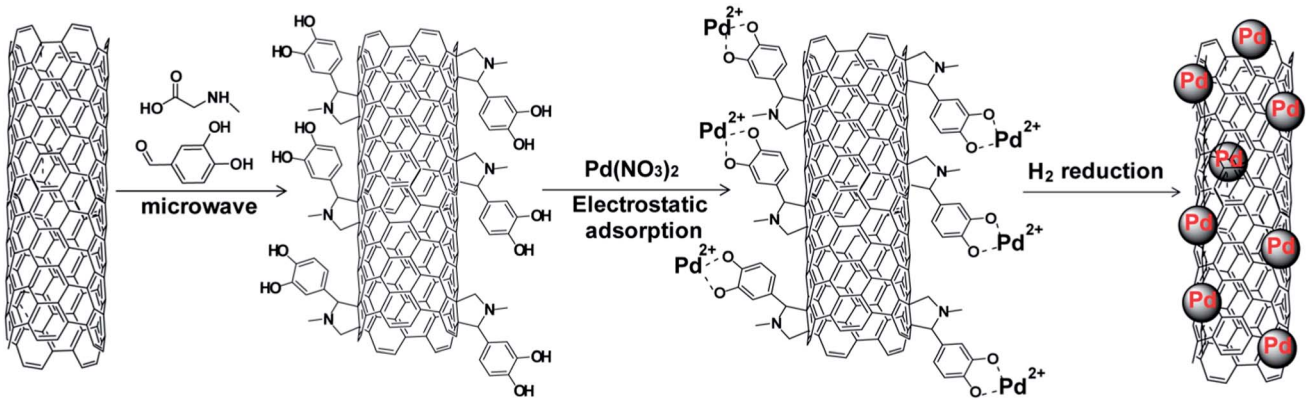

Fig. 2 Schematic view of the process of anchoring Pd NPs onto CNTs.

Table 1 Summary of characterization results

	XPS (at.%)						
Sample	C	N	O	Δm^b (wt%)	S_{BET} (m^2 g^{-1})	–OH/nm^{2c}	I_D/I_G
NF-CNT	99.23	—	0.77		220.5		2.61
CNT-160	96.96	0.68(0.48[a])	2.36	2.46	171.7	2.8	2.55
CNT-200	93.91	0.98(0.75[a])	5.11	5.72	170.4	4.2	2.43
CNT-220	93.58	1.06(0.78[a])	5.36	7.03	176.7	4.4	2.39

[a] The atomic percentage of nitrogen in carbamate bonds was calculated based on the curve fitted N 1s XPS. [b] Δm was obtained by subtracting the weight loss of the non-functionalized CNTs. [c] The number of hydroxyl groups per square nm was calculated based on the values of the atomic percentage of nitrogen in carbamate bonds and specific surface area.

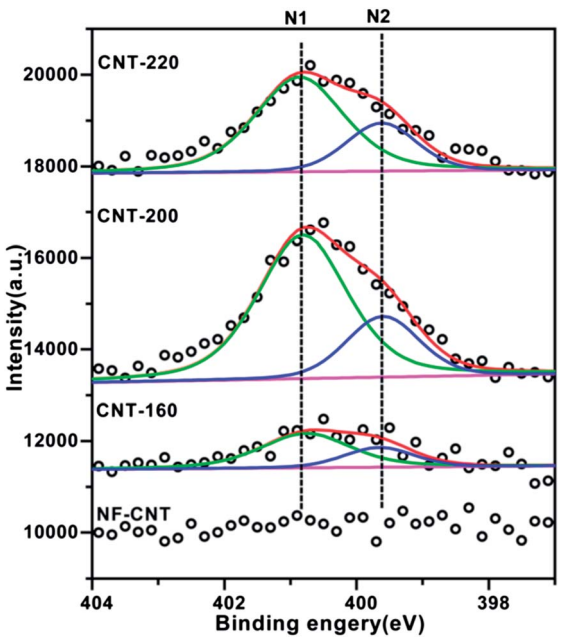

Fig. 4 The curve fitted N 1s XPS of NF-CNT, CNT-160, CNT-200 and CNT-220.

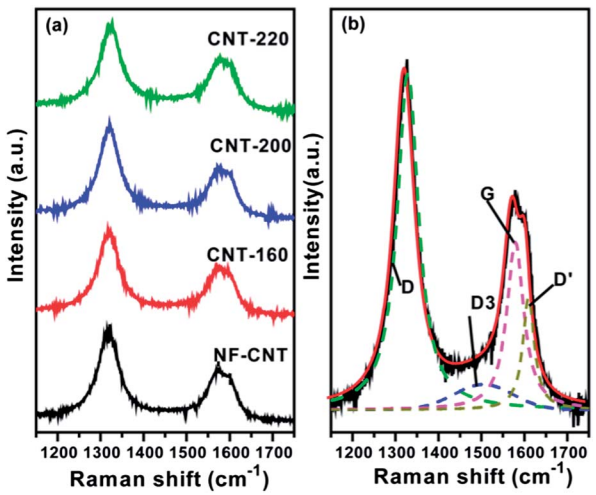

Fig. 5 (a) The Raman spectra of CNT samples, and the fitting of the Raman spectra of the NF-CNT sample.

O3), as shown in Fig. S1 and S2.† We found that the relative intensities of C2 and O3 increased with the increase of reaction temperature, indicating that the content of the phenolic hydroxyl groups could be adjusted by changing the reaction temperature (Table S1†).

The CNT functionalization was further verified using Raman spectroscopy. The Raman bands of samples and the quantitative results are summarized in Fig. 5 and Table S2.† The Raman spectra of non-functionalized and functionalized CNT samples were deconvoluted and fitted using three Lorentzian peaks centered at 1320 cm^{-1}, 1570 cm^{-1}, and 1602 cm^{-1}, and a Gaussian peak centered at 1500 cm^{-1} (assigned to D, G, D′ and D3 bands) according to the reported literature.[11] It is well-known that the D band centered at *ca.* 1320 cm^{-1} is usually associated with defects and amorphous carbon impurities of CNTs, and the G band centered at *ca.* 1570 cm^{-1} is attributed to the in-plane E_{2g} zone-center mode, *i.e.*, the ordered sp^2 hybridized carbon network.[12,13] The D′ band around 1602 cm^{-1} is assigned to the lattice vibration of several graphene layers or small graphite domains on bulk graphite crystals, which usually appears in defective graphite.[11a] The intensity ratio of D and G bands (I_D/I_G) was used to probe the degree of functionalization.[4b] As shown in Table 1, the value of I_D/I_G decreased from 2.61 of non-functionalized CNTs to 2.39 of CNT-220, indicating that the functionalization reaction was proceeded through the covalent bonding with the diffuse defect sites of CNTs.[4b] However, the variation of the I_D/I_G ratio is not significant with respect to the non-functionalized CNTs.

In addition, the surface area and pore structure of CNTs were characterized using nitrogen adsorption. Although the surface area of functionalized CNTs decreased (Table 1), the nitrogen adsorption–desorption isotherms (Fig. 6) between non-functionalized CNTs and functionalized ones were very similar, which showed a typical hysteresis attributed to a mesoporous structure. The similarity of nitrogen adsorption–desorption isotherms of CNTs indicated that the structure of CNTs was not damaged heavily after the functionalization, which was in agreement with Raman results. Finally, the surface concentration of phenolic hydroxyl groups (hydroxyl groups per square nanometer) was calculated according to the atomic percentage of nitrogen in carbamate bonds, combining the results of nitrogen adsorption (Table 1).

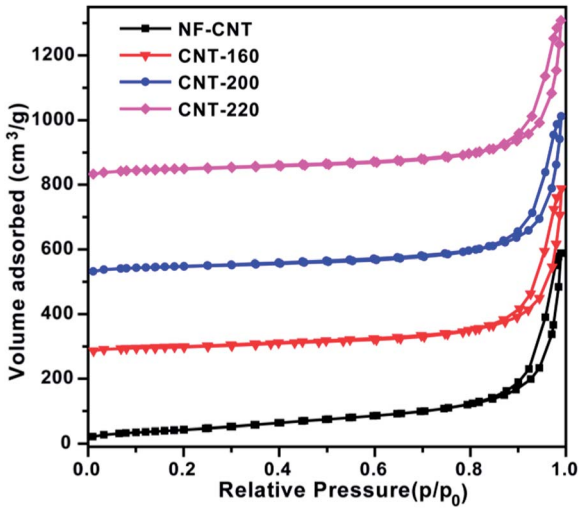

Fig. 6 The nitrogen adsorption–desorption isotherms of non-functionalized and functionalized CNTs. (The isotherms for NF-CNT, CNT-160, CNT-200 and CNT-220 are offset vertically by −20, 250, 500 and 800 $cm^3\ g^{-1}$, respectively.)

Pd NP/CNT nanocomposites

In order to exhibit the superiority of functionalized CNTs as supports, the Pd NP/CNT nanocomposites were prepared by means of strong electrostatic adsorption (Fig. 2). CNT-220 was chosen as a typical functional CNT because of its high functionalization degree. It is well known that the surface properties of CNTs usually affect the Pd dispersion and particle size.[14] When the strong electrostatic adsorption method is used in the catalyst preparation, it is very important to study the point of zero charge (PZC) of the support. By measuring the zeta potential as a function of pH, the acidity or basicity of the CNT surface and the isoelectric point can be determined. As shown in Fig. 7, the PZC of CNT-220 is lower than that of NF-CNT. When the pH was at 4–5, there would be more negative charges on the surface of CNT-220, which was beneficial to anchor the positively charged metal precursors. In this work, we chose Pd $(NO_3)_2$ as metal sources and NF-CNTs as control supports. The nanocomposites were synthesized under the condition of pH = 4–5, followed by reduction with H_2 at 200 °C for 2 h. The final products are denoted as Pd NP/NF-CNT and Pd NP/CNT-220, respectively.

Furthermore, the morphology and structure of the as-synthesized Pd NP/CNT nanocomposites were characterized by transmission electron microscopy (TEM) and high-angle annular dark-field scanning transmission-electron microscopy (HAADF-STEM). The TEM image showed that there were serious agglomerations of Pd NPs with a broad size distribution for NF-CNT (Fig. 8a). This was because the small amount of functional groups on the surface of NF-CNT led to the weak interactions between Pd precursors and CNTs, as a result, Pd NP agglomeration occurred at the reduction process.In contrast, Pd NPs in Pd NP/CNT-220 were much more uniform and the average size of Pd NPs was approximately 1.5 ± 0.4 nm as shown in Fig. 8b and c. Moreover, the HAADF-STEM image (Fig. 8d) further proved the homogeneity of Pd NPs supported on CNT-220. In addition, the ICP measurement confirmed that the Pd loading in Pd NP/CNT-220 was higher than that in Pd NP/NF-CNT (1.69 wt% *vs.* 1.15 wt%), which might be also ascribed to the different amounts of surface functional groups on these two supports. The phenolic hydroxyl groups not only can improve the dispersion of CNTs in an aqueous phase, but also can prevent Pd NPs from agglomerating. Furthermore, the color change of Pd precursor solutions before and after immobilization could explain the results. In the case of CNT-220, the solution color turned transparent after supporting, in contrast, a light yellow color was observed after Pd supported on NF-CNT (Fig. S3†).

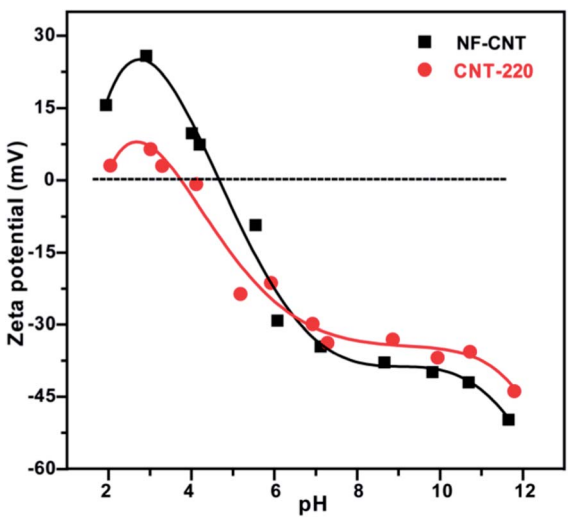

Fig. 7 The Zeta potential of NF-CNT and CNT-220 at varying pHs.

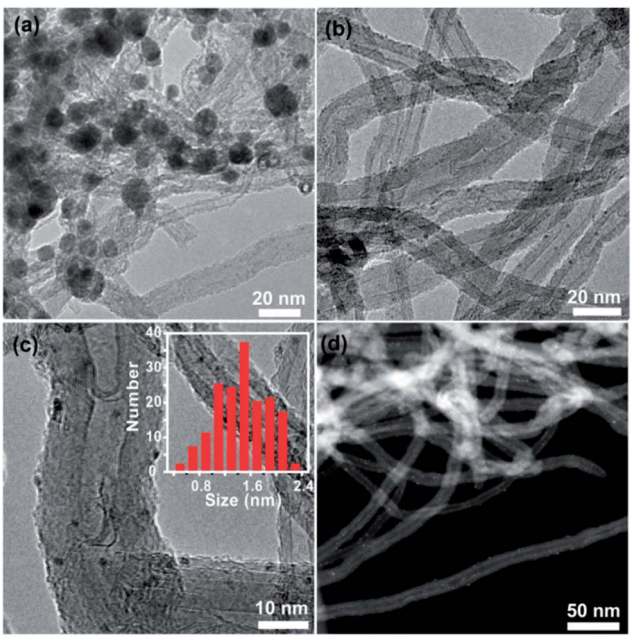

Fig. 8 (a) The TEM images of Pd NP/NF-CNT nanocomposites, (b and c) TEM and (d) HAADF-STEM images of Pd NP/CNT-220 nanocomposites. Insets in (c) show the size distribution of Pd nanoparticles.

To further reveal the superiority of the proposed functionalization method, concentrated HNO_3 oxidized CNTs (O-CNT) were used as supports to make a comparison, and the resulting nanocomposites are denoted as Pd NP/O-CNT. There were various surface functional groups on the surface of O-CNT, mainly carboxyl groups. So, there would be more negative charges on the surface of O-CNT than that of CNT-220 when the pH value was adjusted to 4–5 (Fig. S4†). These factors can also improve the solubility of CNTs in water and enhance the interaction between Pd precursors and CNT supports. However, the particle size and loading of Pd in Pd NP/O-CNT were inferior to those of Pd NP/CNT-220 nanocomposites (Fig. S5†). The reason was ascribed to the difference of the surface functional groups, which played an important role in catalyst preparation. It had been reported that the bonding between Pd clusters and phenolic hydroxyl groups was stronger than that of Pd clusters and carboxyl groups.[14] These results indicated that it was important for the functionalization of CNTs with specific functional groups. Furthermore, the particle size of Pd NPs was also dependent upon the chemical groups on the surface of CNTs. In order to gain more insight into the interaction between Pd with CNTs, the XPS measurements of Pd 3d core level spectra were carried out. As shown in Fig. S6 and Table S3,† Pd $3d_{5/2,3/2}$ peaks observed at 335.7 and 341 eV are ascribed to the Pd metal only, whereas peaks at 337.8 and 343.2 eV correspond to Pd $3d_{5/2,3/2}$ peaks of oxidized Pd–O species.[15] The relative intensity of Pd^{2+} from Pd 3d core level spectra in Pd NP/CNT-220 is higher than that of Pd NP/NF-CNT and Pd NP/O-CNT (18.7% *vs.* 13.1% and 16.6%), which may be attributed to the stronger interaction between palladium species and phenolic hydroxyl groups.

Catalytic performance

To evaluate the catalytic activity of Pd NPs supported on various CNTs,[16–18] the reduction of 4-nitrophenol (4-NP) to 4-aminophenol (4-AP) was chosen as a probe reaction. It is well known that this reaction can be catalyzed by Pd nanoparticles at room temperature and the reaction process can be easily monitored *in situ via* UV/vis spectroscopy.[19] As shown in Fig. 9a, the intensity of the absorbance peak at 400 nm, which could be assigned to 4-NP, gradually decreased with the increase of reaction time. Meanwhile, the intensity of a new absorbance peak at 300 nm increased, which was attributed to 4-AP. The reaction finished within 7 min. According to the reported literature,[20] the kinetic equation of the reduction of 4-NP can be expressed as:

$$-\frac{\partial C_t}{\partial t} = k'[\mathrm{NaBH_4}]^m (C_t)^n \quad (1)$$

where m and n are the reaction order of $[NaBH_4]$ and [4-NP], respectively. C_t is the concentration of 4-NP at the time of t, and k' is the rate constant. Because the concentration of $NaBH_4$ is in great excess compared to that of 4-NP, eqn (1) can be simplified as follows:

$$-\frac{\partial C_t}{\partial t} = k\ (C_t)^n \quad (2)$$

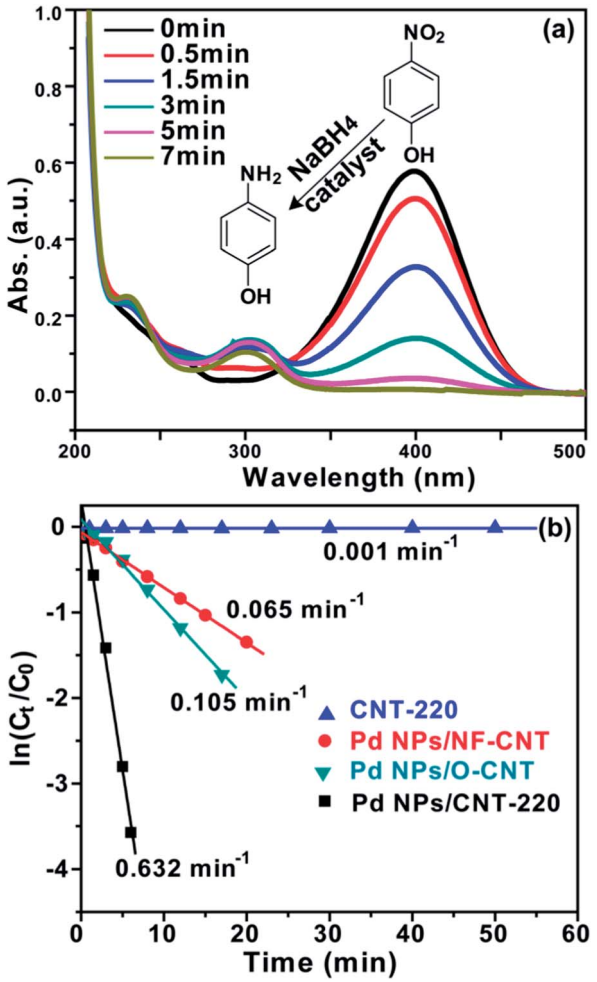

Fig. 9 (a) The time-dependent absorption spectra of the reaction solution in the presence of the Pd NP/CNT-220 nanocomposites; (b) the plot of $\ln(C_t/C_0)$ *versus* time for the reduction of 4-NP using different catalysts.

$$\ln\left(-\frac{\partial C_t}{\partial t}\right) = n \ln(C_t) + \ln k \quad (3)$$

According to the linear regression analysis of the $\ln(-\partial C_t/\partial t)$ *versus* $\ln(C_t)$ plot, the value of n can be given, $n = 0.90 \pm 0.05$, indicating that the reaction belongs to the pseudo-first-order reaction kinetics with respect to 4-NP (Fig. S7†). Then, eqn (3) becomes:

$$\ln(C_t/C_0) = -kt \quad (4)$$

where C_0 is the initial concentration of 4-NP and k is the rate constant. Therefore, a pseudo-first-order reaction kinetics can be applied to determine the reaction rate constant. According to the linear relationship of $\ln(C_t/C_0)$ with t, we can obtain the rate constant of this reaction for the Pd NP/CNT-220 catalyst, that is, k equals to 0.632 min^{-1} and the TOF is 18 min^{-1} (Fig. 9b). In order to elucidate the high catalytic activity of Pd NP/CNT-220, we also performed control experiments using CNT-220, Pd NP/NF-CNT and Pd NP/O-CNT. The catalytic activity of CNT-220

could be neglected due to the rate constant of 0.001 min^{-1}, indicating that Pd NPs were the active sites in this reaction. The Pd NP/NF-CNT showed a lower catalytic activity than Pd NP/CNT-220 (k: 0.065 min^{-1} *vs.* 0.632 min^{-1}), because of a larger particle size and a lower loading of Pd on NF-CNT with respect to CNT-220. Meanwhile, the Pd NP/O-CNT also exhibited lower catalytic activity than Pd NP/CNT-220 (k: 0.105 min^{-1} *vs.* 0.632 min^{-1}), but the catalytic activity of Pd NP/O-CNT was higher than that of the Pd NP/NF-CNT, indicating that the Pd loading and their metal–support interaction depended on the oxygen functional groups on the surface of the CNTs.

Compared to the reported Pd NPs supported on the CNT (6.32 min^{-1} of TOF)[17] and Au NPs immobilized on the mesoporous silica (0.042 min^{-1} of TOF),[18] our catalyst shows significantly improved catalytic activity, due to the lower loading and smaller particle size. After the catalytic reaction, the Pd 3d XPS results of the Pd NP/CNT-220 nanocomposites (Fig. S8 and Table S3†) indicate that the relative intensity of Pd^0 increases from 81.3 to 84.2%, which may be ascribed to Pd^{2+} reduced by $NaBH_4$ during the reaction process.

Conclusions

In summary, CNTs were functionalized successfully *via* 1,3-dipolar cycloaddition reaction under the microwave condition. The surface concentration of phenolic hydroxyl groups on CNTs could be adjusted by tuning the reaction temperature. In addition, we prepared Pd NP/CNT nanocomposites through strong electrostatic adsorption and hydrogen reduction. The results indicated that the functional groups could not only improve the dispersion of CNTs in water, but also enhance the interaction between Pd precursors and CNT supports, which prevented Pd NPs from agglomerating, therefore leading to a uniform dispersion of Pd NPs. Furthermore, the Pd NP/CNT-220 nanocomposites showed a relatively high catalytic activity for the reduction of 4-nitrophenol. The TOF of this catalyst was up to 18 min^{-1}, which is attributed to the small particle size and the uniform distribution. We believe that this method is beneficial to fabricate CNTs with single type of functionalities and the construction strategy can also be applied to introduce other small sized noble metal particles onto CNTs. Meanwhile, this functional method can be applied in other carbon materials, such as fullerenes, graphene and activated carbon, and so on.

Acknowledgements

The authors acknowledge the financial support from MOST (2011CBA00504), NSFC of China (51001098, 21133010, 51221264, 21261160487, 21303226, 21353004), the "Strategic Priority Research Program" of the Chinese Academy of Sciences, grant no. XDA09030103, a General Financial Grant from the China Postdoctoral Science Foundation (2012M520651) and the open project of the State Key Laboratory of Urban Water Resource and Environment (no. QA201023). We also thank Mr Bingwei Zhong, Mr Shuchang Wu and Mr Jia Wang for fruitful discussions.

Notes and references

1 (*a*) P. Weerachawanasak, O. Mekasuwandumrong, M. Arai, S. I. Fujita, P. Praserthdam and J. Panpranot, *J. Catal.*, 2009, **262**, 199; (*b*) X. F. Guo, D. Y. Jang, H. G. Jang and G. J. Kim, *Catal. Today*, 2012, **186**, 109; (*c*) S. S. Stahl, *Angew. Chem., Int. Ed.*, 2004, **43**, 3400; (*d*) K. Gong, D. Su and R. R. Adzic, *J. Am. Chem. Soc.*, 2010, **132**, 14364; (*e*) R. Arrigo, S. Wrabetz, M. E. Schuster, D. Wang, A. Villa, D. Rosenthal, F. Girsgdies, G. Weinberg, L. Prati, R. Schlögl and D. S. Su, *Phys. Chem. Chem. Phys.*, 2012, **14**, 10523.

2 (*a*) C. Zhu and S. J. Dong, *Nanoscale*, 2013, **5**, 10765; (*b*) J. Kang, O. L. Li and N. Saito, *Nanoscale*, 2013, **5**, 6874; (*c*) H. Li and J. J. Cooper-White, *Nanoscale*, 2013, **5**, 2915.

3 (*a*) R. H. Baughman, A. A. Zakhidov and W. A. de Heer, *Science*, 2002, **297**, 787; (*b*) P. J. F. Harris, *Carbon Nanotube Science: Synthesis, Properties and Applications*, Cambridge Univeristiy press, 2009.

4 (*a*) M. C. Paiva, F. Simon, R. M. Novais, T. Ferreira, M. F. Proença, W. Xu and F. Besenbacher, *ACS Nano*, 2010, **4**, 7379; (*b*) G. Grassi, A. Scala, A. Piperno, D. Iannazzo, M. Lanza, C. Milone, A. Pistone and S. Galvagno, *Chem. Commun.*, 2012, **48**, 6836; (*c*) B. Gebhardt, Z. Syrgiannis, C. Backes, R. Grauper, F. Hauke and A. Hirsch, *J. Am. Chem. Soc.*, 2011, **133**, 7985.

5 (*a*) N. Karousis and N. Tagmatarchis, *Chem. Rev.*, 2010, **110**, 5366; (*b*) P. Singh, S. Campidelli, S. Giordani, D. Bonifazi, A. Bianco and M. Prato, *Chem. Soc. Rev.*, 2009, **38**, 2214.

6 Y. T. Kim and T. Mitani, *J. Catal.*, 2006, **238**, 394.

7 V. Georgakilas, A. Bourlinos, D. Gournis, T. Tsoufis, C. Trapalis, A. Mateo-Alonso and M. Prato, *J. Am. Chem. Soc.*, 2008, **130**, 8733.

8 (*a*) Y. Wang, Z. Iqbal and S. Mitra, *Carbon*, 2005, **43**, 1015; (*b*) F. G. Brunetti, M. A. Herrero, J. de M. Muñoz, A. Díaz-Ortiz, J. Alfonsi, M. Meneghetti, M. Prato and E. Vázquez, *J. Am. Chem. Soc.*, 2008, **130**, 8094.

9 G. Beamson and D. Briggs, High Resolution of Organic Polymers, in *The Scienta ESCA 300 Database*, J. Wiley & Sons, Chichester, UK, 1992, appendix 4.

10 (*a*) R. J. J. Jansen and H. van Bekkum, *Carbon*, 1995, **33**, 1021; (*b*) R. Arrigo, M. Hävecker, S. Wrabetz, R. Blume, M. Lerch, J. McGregor, E. P. J. Parrott, J. A. Zeitler, L. F. Gladden, A. Knop-Gericke, R. Schlögl and D. S. Su, *J. Am. Chem. Soc.*, 2010, **132**, 9616; (*c*) C. M. Chen, Q. Zhang, X. C. Zhao, B. Zhang, Q. Q. Kong, M. G. Yang, Q. H. Yang, M. Z. Wang, Y. G. Yang, R. Schlögl and D. S. Su, *J. Mater. Chem.*, 2012, **22**, 14076; (*d*) G. L. Tian, M. Q. Zhao, Q. Zhang, J. Q. Huang and F. Wei, *Carbon*, 2012, **50**, 5323; (*e*) W. Qi, W. Liu, B. Zhang, X. Gu, X. Guo and D. S. Su, *Angew. Chem., Int. Ed.*, 2013, **52**, 14224.

11 (*a*) A. Sadezky, H. Muckenhuber, H. Grothe, R. Niessner and U. Pöschl, *Carbon*, 2005, **43**, 1731; (*b*) A. Rinaldi, J. Zhang, B. Frank, D. S. Su, S. B. A. Hamid and R. Schlögl, *ChemSusChem*, 2010, **3**, 254.

12 S. Osswald, E. Flahaut and Y. Gogotsi, *Chem. Mater.*, 2006, **18**, 1525.

13 Y. Zhang, H. He, C. Gao and J. Wu, *Langmuir*, 2009, **25**, 5814.
14 T. Xu, Q. Zhang, H. Yang, X. Li and J. Wang, *Ind. Eng. Chem. Res.*, 2013, **52**, 9783.
15 (*a*) X. Chen, Y. Hou, H. Wang, Y. Cao and J. He, *J. Phys. Chem. C*, 2008, **112**, 8172; (*b*) G. B. Hoflund, H. A. E. Hagelin, J. F. Weaver and G. N. Salaita, *Appl. Surf. Sci.*, 2003, **205**, 102; (*c*) S. Santra, P. K. Hota, R. Bhattacharyya, P. Bera, P. Ghosh and S. K. Mandal, *ACS Catal.*, 2013, **3**, 2776; (*d*) S. Santra, P. Ranjan, P. Bera, P. Ghosh and S. K. Mandal, *RSC Adv.*, 2012, **2**, 7523.
16 (*a*) Z. Jin, M. Xiao, Z. Bao, P. Wang and J. F. Wang, *Angew. Chem., Int. Ed.*, 2012, **51**, 6406; (*b*) B. C. Yang, C. M. Zhao, M. D. Xiao, F. Wang, C. H. Li, J. F. Wang and J. C. Yu, *Small*, 2013, **9**, 1003.
17 H. Li, L. Han, J. J. Cooper-White and I. Kim, *Green Chem.*, 2012, **14**, 586.
18 Y. Deng, Y. Cai, Z. Sun, J. Liu, C. Liu, J. Wei, W. Li, C. Liu, Y. Wang and D. Zhao, *J. Am. Chem. Soc.*, 2010, **132**, 8466.
19 (*a*) M. Schrinner, M. Ballauff, Y. Talmon, Y. Kauffmann, J. Thun, M. Moller and J. Breu, *Science*, 2009, **323**, 617; (*b*) J. Zeng, Q. Zhang, J. Chen and Y. N. Xia, *Nano Lett.*, 2010, **10**, 30.
20 J. Huang, Y. Zhu, M. Lin, Q. Wang, L. Zhao, Y. Yang, K. X. Yao and Y. Han, *J. Am. Chem. Soc.*, 2013, **135**, 8552.